2018 IEEE International Conference on Systems, Man, and Cybernetics

Total variation regularized low-rank tensor approximation for color image denoising

Yongyong Chen and Yicong Zhou*
Department of Computer and Information Science
University of Macau, Macau 999078, China
Email: YongyongChen.cn@gmail.com, yicongzhou@umac.mo

***Abstract*—Existing approaches for low-rank approximation either need a rank prior or ignore the spatial smooth characteristic of a color image. To overcome these drawbacks, we propose a total variation regularized low-rank tensor approximation model for color image denoising. The model integrates the strong low-rank prior into a tensor-SVD framework, and introduces the hyper total variation to model the spatial smooth structure of images. Using the alternating direction method of multipliers, we propose a simple algorithm to solve our model. Extensive results on simulated and real noisy color images demonstrate the better performance of the proposed method against state-of-the-art denoising methods.**

***Index Terms*—Low-rank tensor approximation, tensor-singular value decomposition, color image denoising.**

I. Introduction

Exploiting low-dimensional structure from high-dimensional data, namely, low-rank matrix/tensor approximation [1], [2], has received increasing attention. However, during the image acquisition and transmission procedures, images are inevitably corrupted by noise. This poses great challenges to further applications, such as image inpainting, image classification and objection detection. Therefore, image denoising becomes a fundamental problem.

Due to the presence of noise, the observed images may not exhibit low-rank property. The core of image denoising task in recent efforts [1]–[7] is how to exactly build a proper low-rank regularizer to model the global structure of the underlying image. As the important work for low-rank matrix approximation (LRMA) [1], Candès *et al.* proposed a robust principal component analysis (RPCA) model. It measures the error (including outliers, gross corruptions) using l_1-norm, leading to the following convex formulation:

$$\min_{L,S} \|L\|_* + \lambda\|S\|_1 \quad s.t. \quad L + S = Y, \tag{1}$$

where λ is a non-negative regulairzing parameter. $\|L\|_*$, known as the nuclear norm, is defined as the sum of singular values of L. Then, the noisy observation Y is decomposed into a low-rank term L and a sparse component S. RPCA can be regarded as a robust version of PCA which applies the l_2-norm to measure the error. However, because l_2-norm is optimal to suppress additive Gaussian noise, PCA is sensitive to impulse noise. Although the model in (1) can obtain the global solution under the theoretical guarantee, many works have proven that non-convex low-rank approximations could achieve further boosting performance for image recovery. For instance, Gu *et al.* [4] adopted the weighted strategy to the nuclear norm, namely the weighted nuclear norm, and found that it is closer to the original rank function than the nuclear norm. This is mainly due to the striking fact that, no matter how big a singular value is, the contribution of this one for the rank function should be 1. Nonetheless, a big challenge is how to set a proper weight for each singular value. Different from the weighted idea, a new non-convex LRMA using the Laplace function was proposed in [5] with promising empirical performance for image denoising [6].

To handle the tensor data, these above methods must unfold the tensor data along mode-3 to produce the matrix Y. This is insufficient and may cause loss of useful information along other two dimensions [2]. Thus, these approaches are able to handle only the matrix data. Recent advances [2], [8], [9] have investigated that tensor-based methods have great potential in image denoising task. However, the tensor rank is difficult to define and implement in real applications. Different tensor decompositions have different tensor ranks. For example, CANDECOMP/PARAFAC (CP) [10] decomposes a tensor into a number of rank-1 factors. Then the CP rank is defined as the smallest number of rank-1 factors. As a result, it may suffer from high computation cost and its best low-rank approximation is unknown because it is intractable to compute the CP rank [2]. Another way to reveal the algebraic structure is Tucker decomposition [12] decomposing a tensor data into one small core tensor and a set of matrices [2], [11]. However, the ranks along all modes must be predefined by human before running the algorithm. This may be difficult in practice. Most of the aforementioned methods for image denoising are based on the low-rank prior that models the high correlation between channels or patches, without consideration of the local piecewise smooth structure of an image.

To overcome these drawbacks, in this paper we propose the Total Variation-regularized Low-rank Tensor approximation (TVLT) model. The total variation is a perfect regularizer for preserving edge information and the local piecewise smoothness. The proposed TVLT is a unified framework that takes two priors into consideration for color image denoising: global low-rank property and local piecewise smooth characteristic. Specifically, we first utilize the tensor nuclear norm based on the recently proposed tensor-SVD framework [10], [11] to model the low-rank prior. Then, we leverage the tensor RPCA to analyze the color image with automatical determination of

2577-1655/18/$31.00 ©2018 IEEE
DOI 10.1109/SMC.2018.00432

the tensor rank. Moreover, the noisy color image is treated as a tensor data to make fully advantage of correlations along different channels. It is decomposed into a low tubal rank tensor term, a sparse component, and a tensor data. Furthermore, we propose an easy-to-implement algorithm based on the alternating direction method of multipliers (ADMM). Lastly, extensive experiments on simulated and real noisy color images validate the effectiveness of our method qualitatively and quantitatively.

II. Proposed TVLT model

This section first introduces the TVLT model that integrates the tensor tubal norm, l_1-norm, and TV regularization in a unified framework, and then proposes an algorithm to use ADMM to solve the TVLT model.

A. TVLT model

For an observed noisy color image $\mathcal{Y}$ of size $\mathbf{R}^{m\times n\times 3}$, let $\mathcal{L}$ be the desired unknown color image to be recovered. Then, the denoising task is to estimate $\mathcal{L}$ from $\mathcal{Y}$ satisfying the following linear superimposition:

$$\mathcal{L}+\mathcal{S}+\mathcal{G}=\mathcal{Y}, \tag{2}$$

where $\mathcal{S}$, $\mathcal{G}$ correspond to impulse noise, and Gaussian noise, respectively.

Here, we consider two priors of the color images: global low-rank property and local piecewise smooth characteristic, with their corresponding regularizers into model (2), and obtain our final model:

$$\begin{aligned}\min_{\mathcal{L},\mathcal{S},\mathcal{G}}\ & \alpha\|\mathcal{L}\|_{\circledast}+\mu\|\mathcal{L}\|_{HTV}+\lambda\|\mathcal{S}\|_1+\gamma\|\mathcal{G}\|_F^2\\ s.t.\ \ & \mathcal{L}+\mathcal{S}+\mathcal{G}=\mathcal{Y},\end{aligned} \tag{3}$$

where $\alpha,\mu,\lambda,\gamma$ are non-negative parameters. $\|\mathcal{L}\|_{\circledast}$ represents the tensor nuclear norm, which is defined as the sum of singular values of all the frontal slices of $\hat{\mathcal{L}}$[1]. While the second term is the hyper total variation (HTV), defined as:

$$\|\mathcal{L}\|_{HTV}=\sum_{t=1}^{3}\|\mathcal{L}^{(t)}\|_{TV}, \tag{4}$$

where $\mathcal{L}^{(t)},(t=1,2,3)$ is the t-th channel of the color image $\mathcal{L}$. For a given matrix L, the traditional TV norm is defined as $\|L\|_{TV}=\|\nabla_x L\|_1+\|\nabla_y L\|_1$, where operators ∇_x and ∇_y are the finite-difference operators along the x and y dimensions, respectively. Compared with matrix image denoising approaches, such as RPCA in (1), the main advantage of our model is that it can employ not only the high correlation along three channels of color image but also the spatial information. Furthermore, it also explores the smooth structure, *i.e.,* spatial continuity by the HTV norm in a tensor framework. Thus, our method can recover a more accurate color image.

[1]where $\hat{\mathcal{L}}$ is obtained by performing the fast Fourier transformation (FFT) along the tube fibers of $\mathcal{L}$. For more details about tensor nuclear norm may be found in [2], [10], [11].

B. Solution procedures of TVLT

Note that, in the objective function, the first two terms $\|\mathcal{L}\|_{\circledast}$ and $\|\mathcal{L}\|_{HTV}$ are coupled, because they share the same variable $\mathcal{L}$. An intuitive explanation is that we impose both global low-rank and local piecewise smooth priors to the recovered color image. Then, we employ the variable splitting technique [13] to solve our model (3). By introducing the auxiliary variable $\mathcal{Z}$, our proposed TVLT model (3) can be reformulated as the following problem:

$$\begin{aligned}\min_{\mathcal{L},\mathcal{Z},\mathcal{S},\mathcal{G}}\ & \alpha\|\mathcal{L}\|_{\circledast}+\mu\|\mathcal{Z}\|_{HTV}+\lambda\|\mathcal{S}\|_1+\gamma\|\mathcal{G}\|_F^2\\ s.t.\ \ & \mathcal{L}+\mathcal{S}+\mathcal{G}=\mathcal{Y},\quad \mathcal{L}=\mathcal{Z}.\end{aligned} \tag{5}$$

Due to the separable property of objective function in model (5) *w.r.t.* the four variables $\mathcal{L},\mathcal{Z},\mathcal{S},\mathcal{G}$, we consider to solve the model (5) under the ADMM framework. The augmented Lagrangian function is given by:

$$\begin{aligned}L_\rho(\mathcal{L},\mathcal{Z},\mathcal{S},\mathcal{G};\mathcal{W},\mathcal{E})=\alpha\|\mathcal{L}\|_{\circledast}+\mu\|\mathcal{Z}\|_{HTV}+\lambda\|\mathcal{S}\|_1+\\ \gamma\|\mathcal{G}\|_F^2+\frac{\rho}{2}(\|\mathcal{L}+\mathcal{S}+\mathcal{G}-\mathcal{Y}+\frac{\mathcal{W}}{\rho}\|_F^2+\|\mathcal{L}-\mathcal{Z}+\frac{\mathcal{E}}{\rho}\|_F^2),\end{aligned} \tag{6}$$

where $\mathcal{W}$, $\mathcal{E}$ are Lagrange multipliers associated with constraints $\mathcal{L}+\mathcal{S}+\mathcal{G}=\mathcal{Y}$ and $\mathcal{L}=\mathcal{Z}$, respectively. ρ is the penalty parameter.

With simple manipulations, we have the following iterative scheme to solve the TVLT model using the general ADMM framework:

1) ***Update $\mathcal{L}$: Restoration****:* Fixing other variables except $\mathcal{L}$ in (6), we can obtain the following sub-problem:

$$\begin{aligned}\mathcal{L}_{k+1}&=\arg\min_{\mathcal{L}} L_{\rho_k}(\mathcal{L},\mathcal{Z}_k,\mathcal{S}_k,\mathcal{G}_k;\mathcal{W}_k,\mathcal{E}_k)\\ &=\arg\min_{\mathcal{L}}\frac{\alpha}{\rho_k}\|\mathcal{L}\|_{\circledast}+\frac{1}{2}\|\mathcal{L}-\mathcal{D}_k\|_F^2,\end{aligned} \tag{7}$$

where $\mathcal{D}_k=\frac{\rho_k(\mathcal{Y}+\mathcal{Z}_k-\mathcal{S}_k-\mathcal{G}_k)-(\mathcal{W}_k+\mathcal{E}_k)}{2\rho_k}$. By the equation $\|\mathcal{L}\|_{\circledast}=\|\mathbf{bdiag}(\hat{\mathcal{L}})\|_*{}^2$, (7) can be transformed into the Fourier domain. It is equivalent to the following formula:

$$\hat{\mathcal{L}}_{k+1}=\arg\min_{\hat{\mathcal{L}}}\frac{\alpha}{\rho_k}\|\mathbf{bdiag}(\hat{\mathcal{L}})\|_*+\frac{1}{2}\|\hat{\mathcal{L}}-\hat{\mathcal{L}}_k\|_F^2; \tag{8}$$

The sub-problem (8) can be separated into 3 independent minimization problems where the t-th problem is

$$\begin{aligned}\hat{\mathcal{L}}_{k+1}^{(t)}&=\arg\min_{\hat{\mathcal{L}}^{(t)}}\frac{\alpha}{\rho_k}\|\hat{\mathcal{L}}^{(t)}\|_*+\frac{1}{2}\|\hat{\mathcal{L}}^{(t)}-\hat{\mathcal{D}}_k^{(t)}\|_F^2\\ &=\Gamma_{\alpha/\rho_k}(\hat{\mathcal{D}}_k^{(t)})\end{aligned} \tag{9}$$

for $t=1,2,3$. $\Gamma_\rho(\mathbf{X})$ is the matrix singular value thresholding operator [15]: $\Gamma_\rho(\mathbf{X}):=\mathbf{U}diag(\bar{\sigma})\mathbf{V}^T$, $\mathbf{X}=\mathbf{U}diag(\sigma)\mathbf{V}^T$ is the SVD of matrix $\mathbf{X}$ and $\bar{\sigma}=\max\{\sigma-\rho,0\}$. Due to the independence of the sub-problems, problem (8) can be efficiently computed in parallel.

2) ***Update $\mathcal{Z}$: Spatial smoothness preservation****:* Fixing other variables except $\mathcal{Z}$ in (6), we can obtain the following sub-problem:

$$\begin{aligned}\mathcal{Z}_{k+1}&=\arg\min_{\mathcal{Z}} L_{\rho_k}(\mathcal{L}_{k+1},\mathcal{Z},\mathcal{S}_k,\mathcal{G}_k;\mathcal{W}_k,\mathcal{E}_k)\\ &=\arg\min_{\mathcal{Z}}\frac{\mu}{\rho_k}\|\mathcal{Z}\|_{HTV}+\frac{1}{2}\|\mathcal{Z}-\mathcal{T}_k\|_F^2,\end{aligned} \tag{10}$$

[2]Please see more details about operator $\mathbf{bdiag}$ in [2], [10], [11].

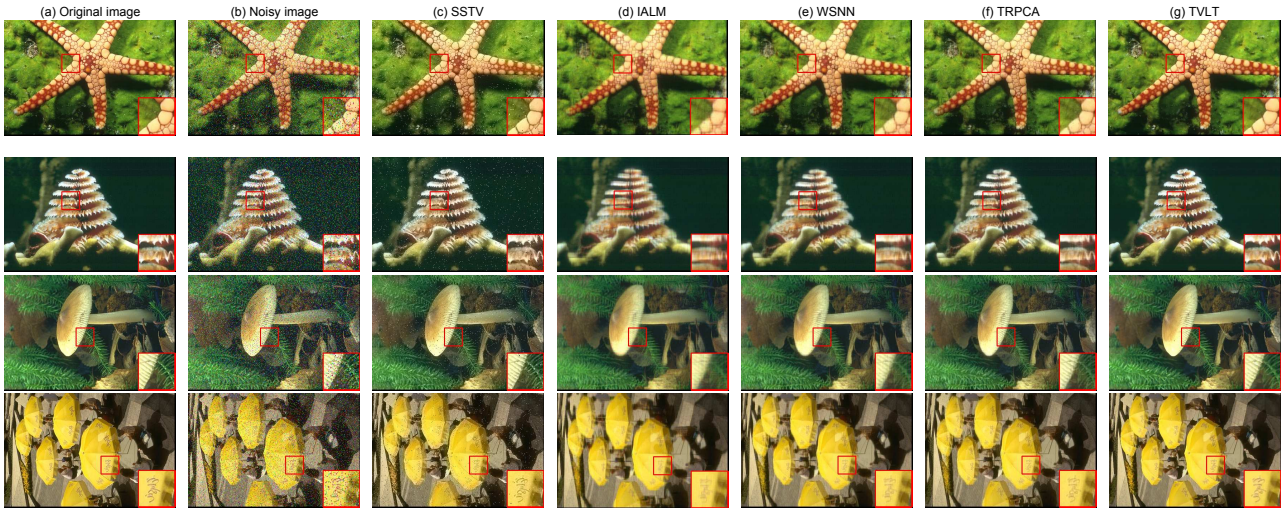

Fig. 1. Denoised results on BSD with 0.1 of impulse noise. Columns from left to right: (a) Original image, (b) Noisy image, the denoised image obtained by (c) SSTV [14], (d) IALM [3], (e) WSNN [9], (f) TRPCA [2], (g) TVLT. The figure is viewed better in zoomed PDF.

where $\mathcal{T}_k = \mathcal{L}_{k+1} + \mathcal{E}_k/\rho_k$. The sub-problem (10) can be split into 3 independent and smaller 2-D total variation regularization problem

$$\mathcal{Z}_{k+1}^{(t)} = \arg\min_{\mathcal{Z}^{(t)}} \frac{\mu}{\rho_k}\|\mathcal{Z}^{(t)}\|_{TV} + \frac{1}{2}\|\mathcal{Z}^{(t)} - \mathcal{T}_k^{(t)}\|_F^2, \quad (11)$$

which can be efficiently solved by a fast gradient-based method [16].

*3) **Update $\mathcal{S}$: Impulse noise removal**:* Fixing other variables except $\mathcal{S}$ in (6), we can obtain the following sub-problem:

$$\begin{aligned}\mathcal{S}_{k+1} &= \arg\min_{\mathcal{S}} L_{\rho_k}(\mathcal{L}_{k+1}, \mathcal{Z}_{k+1}, \mathcal{S}, \mathcal{G}_k; \mathcal{W}_k, \mathcal{E}_k) \\ &= \arg\min_{\mathcal{S}} \frac{\lambda}{\rho_k}\|\mathcal{S}\|_1 + \frac{1}{2}\|\mathcal{S} - \mathcal{M}_k\|_F^2,\end{aligned} \quad (12)$$

where $\mathcal{M}_k = \mathcal{Y} - \mathcal{L}_{k+1} - \mathcal{G}_k - \mathcal{W}_k/\rho_k$. Then the closed-form solution to (12) can be obtained by resorting to the element-wise shrinkage operator, that is,

$$\mathcal{S}_{k+1} = \hbar_{\lambda/\rho_k}(\mathcal{M}_k), \quad (13)$$

and $\hbar_\rho(\mathbf{x}) := sign(\mathbf{x})\max\{|\mathbf{x}| - \rho, 0\}$.

*4) **Update $\mathcal{G}$: Gaussian noise removal**:* Fixing other variables except $\mathcal{G}$ in (6), we can obtain the following sub-problem:

$$\begin{aligned}\mathcal{G}_{k+1} &= \arg\min_{\mathcal{G}} L_{\rho_k}(\mathcal{L}_{k+1}, \mathcal{Z}_{k+1}, \mathcal{S}_{k+1}, \mathcal{G}; \mathcal{W}_k, \mathcal{E}_k) \\ &= \arg\min_{\mathcal{G}} \lambda\|\mathcal{G}\|_F^2 + \frac{\rho_k}{2}\|\mathcal{G} - \mathcal{N}_k\|_F^2,\end{aligned} \quad (14)$$

where $\mathcal{N}_k = \mathcal{Y} - \mathcal{L}_{k+1} - \mathcal{S}_{k+1} - \mathcal{W}_k/\rho_k$. This is a standard least squares regression problem with closed-form solution:

$$\mathcal{G}_{k+1} = (2 * \gamma + \rho_k)^{-1}(\rho_k\mathcal{N}_k). \quad (15)$$

*5) **Update $\mathcal{W}, \mathcal{E}, \rho$: Lagrangian multipliers and penalty parameter**:*

$$\mathcal{W}_{k+1} = \mathcal{W}_k + \rho_k(\mathcal{L}_{k+1} + \mathcal{S}_{k+1} + \mathcal{G}_{k+1} - \mathcal{Y}); \quad (16)$$

$$\mathcal{E}_{k+1} = \mathcal{E}_k + \rho_k(\mathcal{L}_{k+1} - \mathcal{Z}_{k+1}); \quad (17)$$

$$\rho_{k+1} = \min\{\beta * \rho_k, \rho_{max}\}. \quad (18)$$

It is worth noting that we select $\beta > 1$ to further facilitate the convergence speed.

III. Experimental Results

In this section, we conduct experiments on simulated and real noisy color images to show the performance of our TVLT model. All experiments are run in MATLAB R2012a on a 64-bit personal computer with a E5-2609 1.90GHz CPU and 16GB memory.

A. Simulated noisy color image experiment

Compared methods: To validate the performance of our proposed TVLT model, several recent state-of-the-art methods are utilized as baseline methods for color image denoising. They include LRMA based method: IALM [3]; low-rank tensor approximation based methods: TRPCA [2], WSNN [8], [9]; and total variation based method: spatial-spectral total variation (SSTV) [14]. For the IALM method, we applied IALM to each channel of the noisy color image. The parameters α, μ, λ, γ of TVLT are set 0.1, 0.005, $1/\sqrt{3 * 481}$, 0.87 for all simulated situations, respectively.

Quantitative assessment: Except the visual comparison, we also select four commonly quantitative quality indexes, including PSNR, SSIM, FSIM, ERGAS [17] to measure the reconstruction accuracies. In general, an image is closer to the ground truth if it has a higher value of PSNR, SSIM, and FSIM, or lower ERGAS value. We use the Berkeley Segmentation dataset (BSD)[3], including 300 color images of size $321 \times 481 \times 3$. We randomly select 60 images from BSD for this test and each of them is added with different ratios of the salt and pepper noise. The ratios are set to $0.1, 0.2$, respectively. 8 examples of selected images are shown in the first row of Table I.

The denoised results are shown in Figs. 1, 2, and Table I. The best results of each quality index are highlighted in bold. The PSNR, SSIM and FSIM values of all selected images

[3]https://www2.eecs.berkeley.edu/Research/Projects/CS/vision/bsds/

TABLE I
QUANTITATIVE COMPARISON ON 8 BSD COLOR IMAGES WITH 0.1/0.2 OF IMPULSE NOISE.

Methods	Indexes								
Noisy	PSNR	14.39/11.42	16.20/13.18	17.27/14.25	14.80/11.83	14.43/11.42	14.80/12.37	14.89/11.88	14.74/11.74
	SSIM	0.28/0.147	0.296/0.168	0.256/0.146	0.264/0.137	0.19/0.096	0.282/0.149	0.224/0.107	0.268/0.145
	FSIM	0.736/0.589	0.734/0.589	0.682/0.532	0.716/0.568	0.643/0.48	0.74/0.606	0.699/0.558	0.706/0.545
	ERGAS	554.6/780.76	369.24/522.92	329.95/467.28	509.02/716.73	590.79/835.22	385/543.62	522.51/738.18	464.92/656.79
SSTV [14]	PSNR	23.2/17.74	25.09/19.64	25.75/20	23.69/18.75	23.28/17.41	23.69/18.76	23.71/18.13	23.41/18.49
	SSIM	0.76/0.463	0.751/0.462	0.704/0.379	0.742/0.457	0.683/0.335	0.766/0.463	0.712/0.388	0.733/0.452
	FSIM	0.936/0.834	0.928/0.824	0.894/0.761	0.908/0.811	0.884/0.732	0.933/0.83	0.905/0.785	0.906/0.793
	ERGAS	200.68/376.07	132.8/248.44	124.37/240.99	180.75/319.28	213.01/418.31	135.85/260.64	188.84/359.15	174.85/302.25
IALM [3]	PSNR	24.51/23.31	25.65/24.7	24.52/23.88	25.35/24.04	24.18/22.96	25.35/24.41	26.9/25.75	24.93/24.03
	SSIM	0.833/0.757	0.843/0.796	0.822/0.791	0.822/0.754	0.883/0.842	0.783/0.718	0.816/0.749	0.803/0.744
	FSIM	0.886/0.858	0.876/0.855	0.828/0.807	0.881/0.853	0.896/0.875	0.861/0.836	0.864/0.84	0.875/0.851
	ERGAS	171.93/197.19	124.33/138.76	143.35/154.29	152.8/177.06	193.97/223.49	120.51/135.94	130.43/148.77	142.85/158.41
WSNN [9]	PSNR	27.24/25.8	27.92/26.79	26.43/25.44	28.02/26.51	26.84/25.45	28.02/26.59	29.28/27.79	26.9/25.85
	SSIM	0.92/0.868	0.912/0.875	0.888/0.854	0.904/0.849	0.935/0.902	0.893/0.837	0.902/0.844	0.883/0.832
	FSIM	0.938/0.913	0.923/0.902	0.882/0.855	0.929/0.903	0.931/0.912	0.919/0.892	0.917/0.889	0.918/0.894
	ERGAS	125.38/147.76	95.79/109.15	115.15/129.06	110.87/131.35	142.46/167.25	89.98/105.77	99.14/117.64	113.92/128.55
TRPCA [2]	PSNR	29.43/27.5	29.84/28.27	28.78/27.31	29.18/27.32	28.75/27.31	29.18/28.68	30.82/28.94	28.27/26.84
	SSIM	0.95/0.907	**0.946/0.912**	0.932/0.899	0.925/0.868	0.953/0.924	**0.945/0.9**	0.931/0.878	0.913/0.863
	FSIM	0.962/0.939	0.953/0.932	0.928/0.902	0.945/0.918	0.949/0.93	0.958/0.932	0.942/0.914	0.939/0.913
	ERGAS	97.22/121.38	76.97/92.19	88.13/104.25	95.79/118.35	113.88/134.37	66.18/83.18	83.1/103.29	97.23/114.74
TVLT	PSNR	**32.79/29.92**	**32.63/29.84**	**32.89/30.3**	**32.79/30.18**	**36.39/33.35**	**32.79/29.40**	**33.45/30.98**	**31.76/29.37**
	SSIM	**0.955/0.917**	0.945/0.904	**0.96/0.934**	**0.938/0.896**	**0.954/0.936**	0.912/0.864	**0.936/0.893**	**0.927/0.886**
	FSIM	**0.97/0.951**	**0.959/0.935**	**0.962/0.943**	**0.967/0.947**	**0.971/0.961**	**0.96/0.936**	**0.96/0.939**	**0.958/0.939**
	ERGAS	**66.35/92.28**	**55.7/76.83**	**54.66/73.61**	**63.57/85.67**	**47.14/66.77**	**55.63/76.59**	**61.37/81.52**	**65.15/85.82**

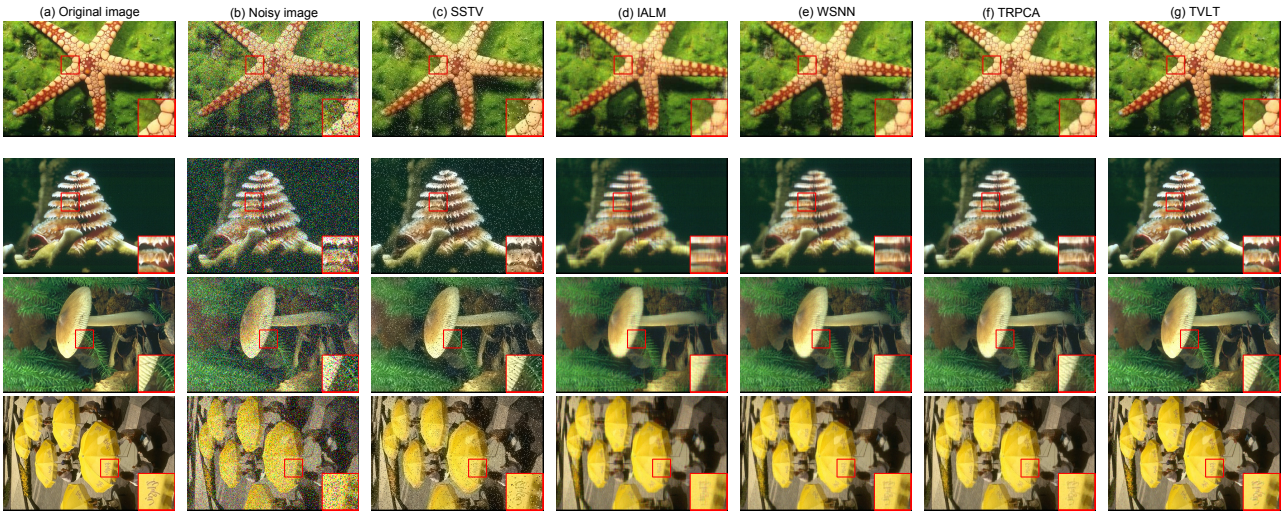

Fig. 2. Denoised results on BSD with 0.2 of impulse noise. Columns from left to right: (a) Original image, (b) Noisy image, the denoising image obtained by (c) SSTV [14], (d) IALM [3], (e) WSNN [9], (f) TRPCA [2], (g) TVLT.

are shown in Fig. 3. As can be seen, for almost all images, TVLT has higher PSNR, SSIM, FSIM and lower ERGAS values and achieves better performance than other competing methods. This is mainly due to the fact that TVLT exploits the global spatial and spectral relationships under the tensor-SVD framework, and the local spatial structure by the total variation regularization. Specially, all other low-rank based methods suffer from the details loss and SSTV cannot fully remove the impulse noise.

B. Real noisy color image experiment

In this subsection, we aim to test the Gaussian noise removal on a real noisy color image: Dog[4], which is mainly contaminated by Gaussian noise. Our TVLT is compared with a basic method: BM3D [19], one blind image denoising method: NC [18], and SSTV [14]. Since there is no ground truth of the real noisy image, the four quantitative indexes cannot be computed. As shown in Fig. 4, one can see that TVLT can reconstruct more details while other methods either partially remove noise or oversmooth the results.

[4]http://www.ipol.im/pub/art/2015/125/

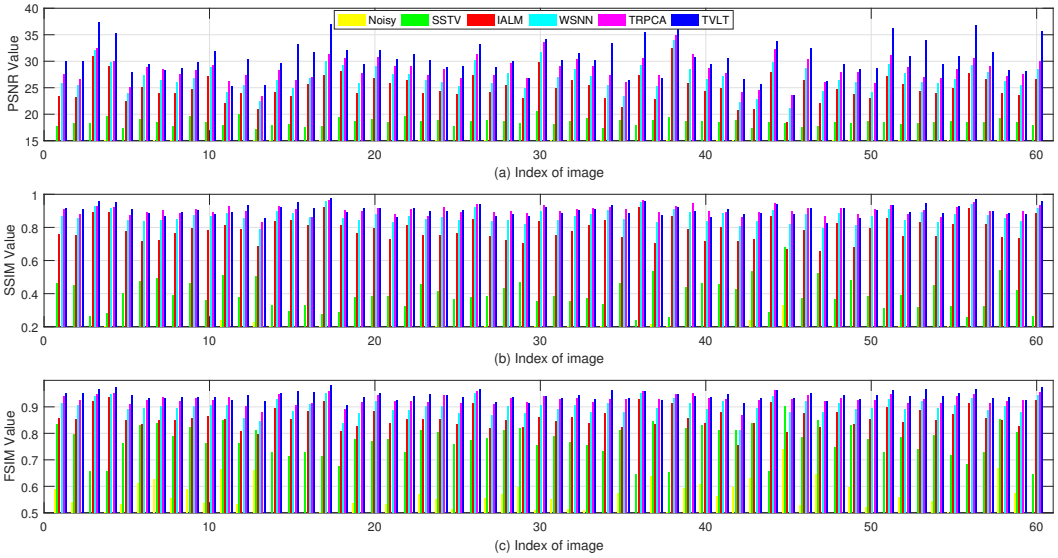

Fig. 3. Comparison of PSNR, SSIM, and FSIM values of different methods for color image denoising on 60 BSD images. (a) PSNR values, (b) SSIM values, and (c) FSIM value. The figure is viewed better in zoomed PDF.

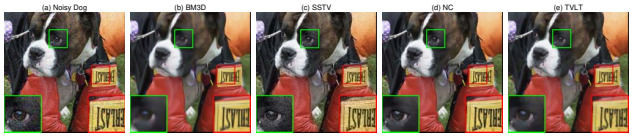

Fig. 4. Denoised results of a real noisy color image. Columns from left to right: (a) Noisy image, and the denoised image obtained by (b) BM3D [19], (c) SSTV [14], (d) NC [18], (e) TVLT. The figure is viewed better in zoomed PDF.

IV. Conclusion

This paper proposed a total variation regularized low-rank tensor approximation method for color image denoising task. The proposed method fully integrates the global and local intrinsic characteristics of the underlying clean color image. Experimental results for impulse and Gaussian noise removal have shown that our proposed method can achieve better performance than several advanced approaches.

V. Acknowledge

This work was supported in part by the Macau Science and Technology Development Fund under Grants FDCT/016/2015/A1 and FDCT/189/2017/A3, and by the Research Committee at University of Macau under Grant MYRG2016-00123-FST.

References

[1] Candes, Emmanuel J., et al. "Robust principal component analysis?." Journal of the ACM (JACM) 58.3 (2011): 11.

[2] Lu, Canyi, et al. "Tensor robust principal component analysis: Exact recovery of corrupted low-rank tensors via convex optimization." Proceedings of the IEEE Conference on Computer Vision and Pattern Recognition. 2016.

[3] Lin, Zhouchen, Minming Chen, and Yi Ma. "The augmented lagrange multiplier method for exact recovery of corrupted low-rank matrices." arXiv preprint arXiv:1009.5055 (2010).

[4] Gu, Shuhang, et al. "Weighted nuclear norm minimization and its applications to low level vision." International Journal of Computer Vision 121.2 (2017): 183-208.

[5] Chen, Yongyong, et al. "Augmented Lagrangian alternating direction method for low-rank minimization via non-convex approximation." Signal, Image and Video Processing 11.7 (2017): 1271-1278.

[6] Chen, Yongyong, et al. "Denoising of Hyperspectral Images Using Nonconvex Low Rank Matrix Approximation." IEEE Transactions on Geoscience and Remote Sensing 55.9 (2017): 5366-5380.

[7] Xu, Fei, et al. "Denoising of Hyperspectral Image Using Low-Rank Matrix Factorization." IEEE Geoscience and Remote Sensing Letters 14.7 (2017): 1141-1145.

[8] Goldfarb, Donald, and Zhiwei Qin. "Robust low-rank tensor recovery: Models and algorithms." SIAM Journal on Matrix Analysis and Applications 35.1 (2014): 225-253.

[9] Huang, Bo, et al. "Provable low-rank tensor recovery." Optimization-Online 4252 (2014): 2.

[10] Kolda, Tamara G., and Brett W. Bader. "Tensor decompositions and applications." SIAM review 51.3 (2009): 455-500.

[11] Zhang, Zemin, et al. "Novel methods for multilinear data completion and de-noising based on tensor-SVD." Proceedings of the IEEE Conference on Computer Vision and Pattern Recognition. 2014.

[12] Tucker, Ledyard R. "Some mathematical notes on three-mode factor analysis." Psychometrika 31.3 (1966): 279-311.

[13] Courant, Richard. "Variational methods for the solution of problems of equilibrium and vibrations." Bulletin of the American mathematical Society 49.1 (1943): 1-23.

[14] Aggarwal, Hemant Kumar, and Angshul Majumdar. "Hyperspectral image denoising using spatio-spectral total variation." IEEE Geoscience and Remote Sensing Letters 13.3 (2016): 442-446.

[15] Cai, Jian-Feng,Candes Emmanuel J., and Shen Zuowei. "A singular value thresholding algorithm for matrix completion." SIAM Journal on Optimization 20.4 (2010): 1956-1982.

[16] Beck, Amir, and Marc Teboulle. "Fast gradient-based algorithms for constrained total variation image denoising and deblurring problems." IEEE Transactions on Image Processing 18.11 (2009): 2419-2434.

[17] Wald, Lucien. "Data fusion: definitions and architectures: fusion of images of different spatial resolutions." Presses des MINES, 2002.

[18] Lebrun, Marc, Miguel Colom, and Jean-Michel Morel. "Multiscale image blind denoising." IEEE Transactions on Image Processing 24.10 (2015): 3149-3161.

[19] Dabov, Kostadin, et al. "Image denoising by sparse 3-D transform-domain collaborative filtering." IEEE Transactions on image processing 16.8 (2007): 2080-2095.